



Calculation model for section strength of moisture-proof layer of wooden building envelope near water area

Wenbo Mao, Aiping Song*

School of Engineering, Yunnan University of Business Management, Kunming 650104, China, email: ynjglxykyc@163.com (A. Song)

Received 3 July 2019; Accepted 20 December 2019

ABSTRACT

The dampness of building envelopes not only poses a great threat to the use and safety of building structures, but also the long-term dampness will affect the aesthetics of the building maintenance structure and even the degradation of indoor air quality, so it is more vulnerable to the offshore. The calculation and simulation of the section strength of the moisture barrier layer of the building envelope structure are of great significance. Based on the analysis of previous research results, this paper takes a moisture-proof layer of wedge-shaped envelope structure as an example, establishes a finite element model through simulation software, simulates the stress loading process and analyzes the stress-strain curve; in the study of steel bar size and steel type After the influence of parameters such as hoop index, concrete strength, water-cement ratio, and reinforcement ratio on the section strength of the moisture-proof layer, combined with the non-linear least-squares method, the shear resistance, bending resistance and compression resistance of the moisture-proof layer of the envelope structure are analyzed, a multi-factor calculation model of strength established. The validity of the model is verified by comparison with experimental data, and it provides a reference for further research.

Keywords: Strength calculation; Moisture barrier; Enclosure structure; Finite element simulation

1. Introduction

The environment in which offshore buildings are located is relatively harsh. It may not only be washed by water flow, wave current, atmospheric corrosion, and freezing and thawing, but also bear the effects of external loads, making the building structure prone to rust, damage, and other resistance changes. It affects the normal use state of the structure and the limit state of the bearing capacity. If condensation occurs on the surface of the wall, it is possible to absorb moisture into the wall by capillary action. Water droplets formed on the surface of the wall are easily found, but the moisture deposited inside the wall is not easily noticeable. The seasonal freezing and thawing process will directly restrict the law of wet and hot migration, which will affect the construction of the project. In particular, the

frost heaving phenomenon will cause destructive crushing stress, which will affect the engineering durability of the building. The dampness of the building envelope not only poses a huge threat to the performance and safety of the building structure but also the long-term dampness will affect the aesthetics of the building maintenance structure and also affect the indoor air quality [1]. Therefore, it is of great significance to calculate and simulate the section strength of the moisture-proof layer of the offshore building envelope which is more susceptible to moisture.

In structural engineering, reinforced concrete columns are the main components of vertical bearing capacity, and their bearing capacity is especially critical, which often determines the safety performance of the overall structural engineering. Damaged damage of reinforced concrete columns usually directly causes damage to the entire structure.

* Corresponding author.

When the building structure shows resistance attenuation, insufficient bearing capacity and weakened function, users tend to be more concerned about the reinforcement and repair of reinforced concrete columns [2]. However, with the increase of steel structure service time, natural aging, damage, corrosion, and other factors have caused the bearing capacity of steel structures to decrease to varying degrees. Therefore, steel structure reinforcement has become an emerging field in today’s construction industry. Because the research on the method of outsourcing concrete reinforced steel is still insufficient, there is no uniform formula for the normal section bearing capacity of the reinforced components. This paper mainly considers the contribution of steel and longitudinal ribs to the bearing capacity by combining the section changing algorithm, and considers. Based on the existing literature, the calculation of the normal section bearing capacity of the reinforced members is derived based on the existing literature, and the reliability of the calculation model is verified by the existing experimental data and simulation data [3].

Based on the previous analysis of the stress and strain tests of reinforced concrete specimens, this paper takes a moisture barrier of a wedge-shaped retaining structure as an example and builds a finite element model through simulation software to simulate various stress loading processes and analyze its stress-strain. Curve; after obtaining the database of the influence of parameters such as steel bar size, steel type, hoop index, concrete strength, water-cement ratio, and reinforcement ratio on the section strength of the moisture-proof layer, the moisture-proof layer of the envelope structure was established by combining nonlinear least squares method, a multi-factor calculation model for section shear, bending, and compressive strength is established. The validity of the model is verified by comparison with experimental data and provides a reference for further research.

2. Establishment of finite element model

2.1. Specimen parameters

The design of the test piece is designed as a reinforced concrete moisture-proof layer with a wedge-shaped retaining structure. The geometrical dimensions are height 600 mm, width 300 mm, span length 2,000 mm, net span

length 1,600 mm; geometric dimensions and reinforcement of the prototype (see Fig. 1). Using C30 strength concrete and material, a total of three sets of height is 500 mm, section width is 160 mm, and section length is 200 mm reinforced rectangular section concrete column, finite element model, each group is set with 0, 1, 2 layers of moisture-proof layer, the boundary conditions are: Apply constraints on three symmetry planes to limit concrete and moisture-proof layer The displacement in the normal direction of the symmetry plane. Model loading method: Set a rigid surface at the top of the column, and set the Coulomb friction between the rigid surface and the rectangular concrete column to consider the hoop effect of the loading plate on the concrete column during the test. In addition, since the mechanism of action between the concrete and the moisture barrier is quite complicated, the frictional unit is set in the concrete and the moisture-proof surface layer to achieve the bonding effect between the two. The concrete cube compressive strength standard value f_{cu} , $K = 30$ MPa, the axial compression and tensile strength design value $f_c = 16.2$ MPa, $f_t = 1.73$ MPa. Shear transfer coefficient of open and closed cracks: $\beta_t = 0.5$, $\beta_c = 0.95$, uniaxial compressive strength is -1 , elastic modulus $E_c = 3 \times 10^4$ MPa, Poisson’s ratio $\nu_c = 0.2$. A concentrated load $P = 80$ MPa is applied at the loading point, and displacement is applied to the bottom surface of the pad at the support.

2.2. Model unit selection

The SOLID65 unit is a unit developed on the basis of the SOLID45 unit. It is specially developed for concrete, rock and other non-uniform materials with a compressive capacity far greater than the tensile capacity. The unit has eight nodes and each node has three degrees of freedom, that is, the linear displacement of the three directions of x , y , and z , and the definition of the reinforcement in three directions [4]. The SOLID65 unit can simulate reinforced steel in concrete and can be used in 3D solid models with or without reinforcement (Fig. 2). This solid model has the properties of crushing and cracking. When simulating reinforced concrete with a limit element, if the SOLID65 unit is used to simulate the concrete, other units are used to simulate the reinforcement. The SOLID65 unit can define up to three different reinforcement materials, the SOLID65 unit can also be used for other aspects of finite element simulation analysis,

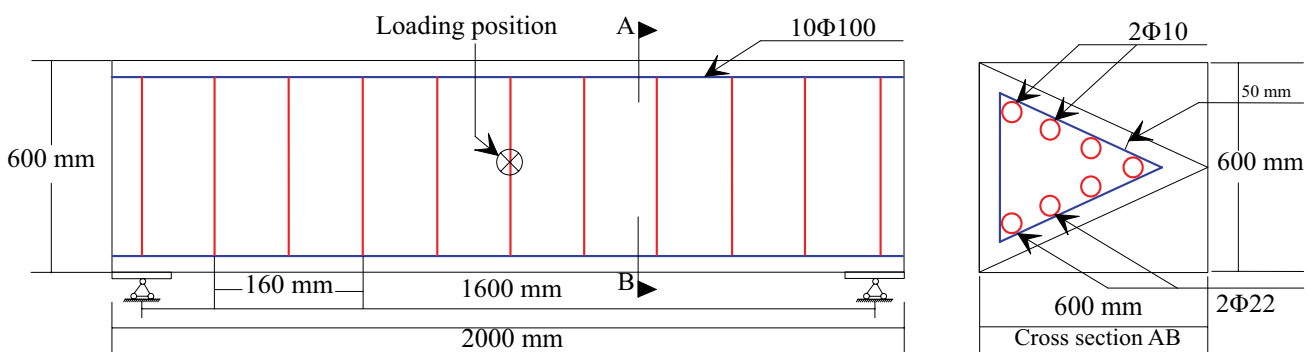


Fig. 1. Specimen geometry and reinforcement.

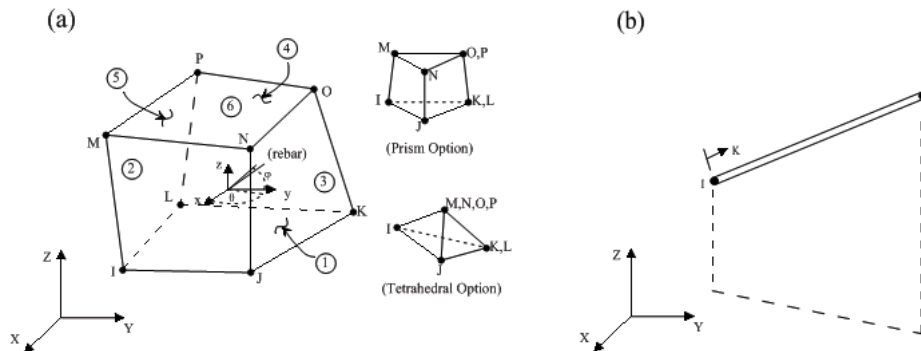


Fig. 2. Schematic diagram of (a) SOLID65 and (b) LINK8 unit [4].

such as geological materials (such as rock) and reinforced composite materials.

Known as the 3D rod unit, the LINK8 unit is a three-dimensional rod unit with a wide range of engineering applications that can be used to simulate trusses, cables, connecting rods, springs, and more. The LINK8 unit can only be subjected to tension or compression. When the pull-only option is used, if the unit is pressed, the stiffness disappears to simulate the slack of the cable or the slack of the chain. This feature is very useful for the static problem of the cable that simulates the entire cable with one unit. It can also be used for dynamic analysis (with inertia or damping effects) when the performance of the slack unit is required, rather than the motion of the slack unit. Each node of the LINK8 unit has three degrees of freedom: translation along the X, Y, and Z directions of the node coordinate system. This unit has plasticity, creep, expansion, stress stiffening, large deformation, large strain, and other work.

2.3. Loading conditions

During the stress loading process of the wedge-shaped moisture-proof layer, the stress concentration is prevented by adding a rigid spacer at the position of the support and the position of the concentrated load. When the displacement constraint is made at the position of the support, one end applies a displacement constraint of three directions to all the nodes on the bottom surface of the pad; the other end applies a displacement constraint of two directions. The concentrated force applied was 80 MPa. For a concentrated load of 80 MPa treated and the solution is forced to 400 load steps, each step is a uniform load of 20 kPa steps until the moisture barrier is destroyed.

3. Stress-strain analysis

3.1. Shear strength

Under the same cement content, the standard value of the compressive strength of the cement soil in the silt formation is reduced by about 30%–40% compared with the strength of the conventional clay; when the cement content is 70%, the cement soil in the silt formation The strength is only 60% of the clay; when the cement content is increased to 20%, although the strength of the cement soil in the silt

formation is significantly improved, it can only reach 50%–60% of the clay. It can be seen from the trend of strength with the time that the strength of cement soil in clay formation is also nonlinear, and the strength growth in the early stage of conservation is 5–7 times higher than that in silt, and the strength growth in the later stage is 1–2 times that of sludge. Considering the difference in performance between conventional clay and sludge, the compressive strength of cement soil in different soil layers should be corrected based on the existing empirical formula. Under the same age and cement content, the standard value of the compressive strength of cement soil in the silt layer is significantly lower than that of the clay soil, and its amplitude is only 60%–90% of the clay soil layer. When the cement content is small, the corresponding cement soil strength is more obvious, only 37%–56% of the clay soil layer. The strength of cement soil in the silt stratum changes with time and the mechanics of silt and clay under the same conditions. The mechanical properties of the silt layer are low, and the parameters such as water content and void ratio of the soil are higher than those of the conventional soil layer. Therefore, the mechanical properties of the soil layer are different from those of the conventional soil layer. Therefore, the data is fitted to the data by using the modified especially limited compressive strength [5–7].

3.2. Bending strength

In the lower load phase, that is, the segment in Fig. 3, it is roughly a straight line, and only at point A, the slope slightly changes. When the load increases to point B, the slip line appears on the surface of the steel pipe. Thereafter, the curve deviates significantly from its initial straight line, and to point C, the load reaches its maximum value and the curve gradually decreases. Before the C point, the test piece was evenly deformed, and the shape was not bent. After point C is exceeded, the shape of the test piece begins to be obviously drummed. If the test continues, after the load drops to point D with the increase of the deformation, it starts to rise again until the new peak point E falls again, and the test piece has been severely deformed. The compressive stress of the concrete gradually decreases until the second stress loss is completed by the tendons. At this time, the compressive stress of the concrete is gradually increased from the compressive stress of the concrete during the use phase. During

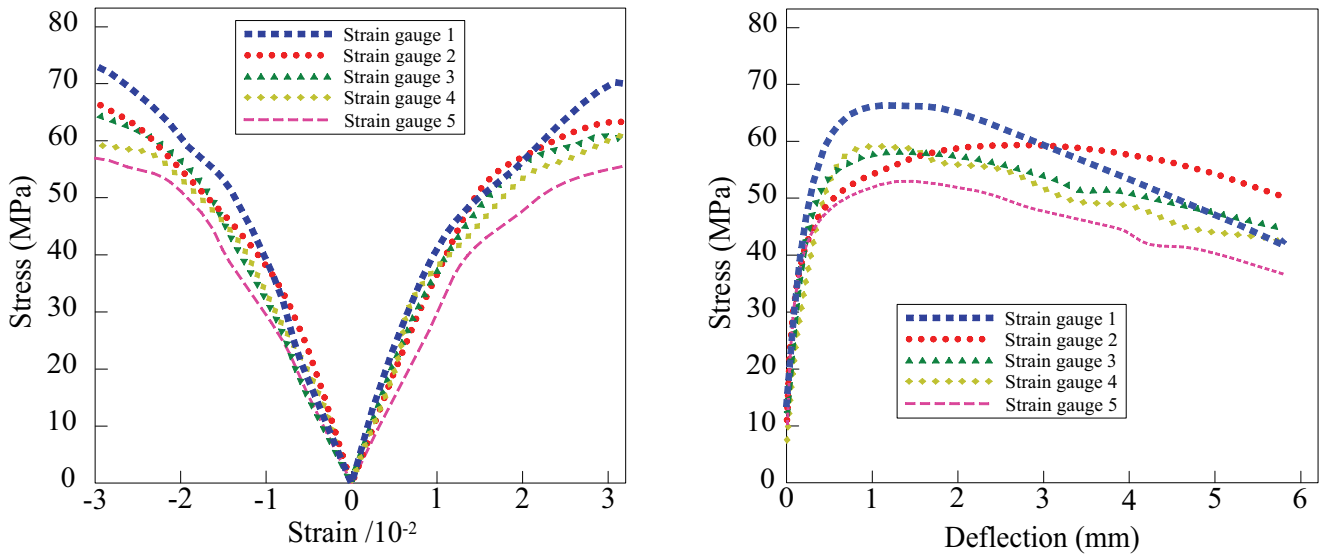


Fig. 3. Stress-strain curves of five different strain gauges.

the construction phase and the use phase, the tensile stress of the tendons gradually decreases. When the compressive stress of the concrete is about to increase to f_c , the tendons are still in the tension state. According to the design experience of pipe piles, the total loss after the second stress loss of the tendons is 20%–40% of the control stress. It is calculated from this that when the compressive stress of the concrete member is reached by an external force, the tensile stress of the tendon is 60%–80% of the control stress.

3.3. Compressive strength

Under the condition of ensuring the internal peeling failure of the concrete at the moisture-proof layer-concrete interface instead of the peeling failure of the rubber layer, the three main influencing factors affecting the peeling bearing capacity of the moisture-proof layer-concrete interface are: concrete strength, width ratio of the moisture-proof layer to concrete surface and length ratio. If the bond strength between the moisture barrier layer and the concrete can be directly determined, the peel load capacity can be obtained by multiplying the bond strength by the bond area of the two. For the test pieces A-1 and B-1, due to the low strength of the concrete, although the concrete interface is not nicked, the internal peeling damage of the concrete occurs. The C-1 test piece is not engraved on the interface because of the high strength of the concrete. In the case of the mark, the peeling damage of the rubber layer and the concrete interface occurs, and the high-strength concrete is not fully exerted, so the C-1 ultimate load is low. For the C-6 test piece, the high-strength concrete interface is subjected to the scoring treatment, and the concrete interior occurs [8]. However, the value of the bond strength has not yet been obtained, and a large number of test results in the test and the existing literature indicate that the concrete strength is the most important factor determining the bond strength of the two. The change of the ratio of the length of the moisture barrier layer to the concrete surface is analyzed for the peeling load of the moisture barrier

layer. It can be seen that with the same parameters, the interfacial peeling bearing capacity increases with the increase of the bond length of the moisture barrier layer; the peeling bearing capacity increases linearly with the increase of the ratio of the moisture barrier layer to the concrete surface.

4. Establishment of strength calculation model

4.1. Multi-factor analysis

The calculated value of the model has the largest error with the experimental value. The error between the calculated value and the experimental value of the model established in this paper is the smallest. This is mainly due to the fact that after the reinforcement is subjected to the secondary load after the steel is yielded, the steel is well plasticized, the component is not damaged, and the new load is transferred to the outer reinforced concrete until it is destroyed (Fig. 4). In the calculation formula of Model 1, the load that can be withstood by the reinforced concrete after the yield of the steel is not taken into account, so the calculated value is small and the error is large, especially when the initial load of the steel is too large, the calculation result is not It has reliability; the calculation formula of model 2, and the calculation formula of the calculation formula established in this paper are in good agreement with the experimental values and can be used as reference calculation models in engineering practice [3]. Due to the existence of longitudinal reinforcement in the outer concrete, the longitudinal reinforcement should bear a certain load when the secondary column is stressed. This makes the bearing capacity of the post-reinforcement column improved. For the convenience of calculation, this paper mainly combines the strength of the combined section. To consider the contribution of the longitudinal reinforcement, the longitudinal reinforcement configuration is finally equivalent to the improvement of concrete strength.

Calculate the vertical distribution of active earth pressure coefficient in the clay layer under different flow directions

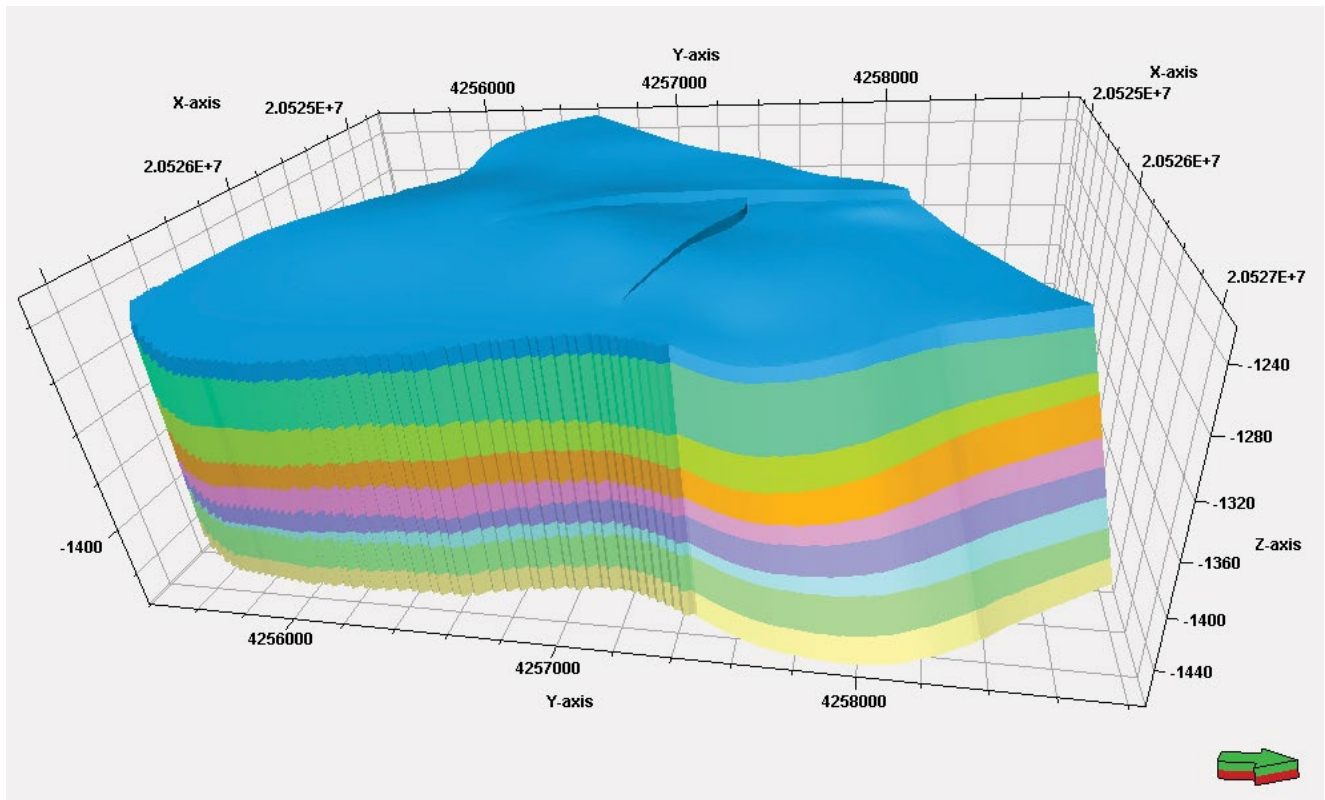


Fig. 4. Deformation state of finite element model after forced loading.

(Fig. 5). Under different flow directions, the active earth pressure coefficient K_a in the homogeneous unsaturated clay layer shows a nonlinear decreasing law with the increase of the depth from the surface, and the decreasing rate decreases with the increase of the surface depth. The main reason for this phenomenon is that the magnitude of the active earth pressure coefficient K_a is positively correlated with the internal friction angle ϕ . For unsaturated soils, the internal friction angle ϕ follows the water content [9]. The active earth pressure coefficient and the active earth pressure intensity are calculated and analyzed. With the increase of surface depth, the active earth pressure coefficient shows a nonlinear decreasing trend. The influence of flow direction on the active earth pressure coefficient is: the active earth pressure coefficient is the smallest when infiltration, the middle is in still water, and the largest in evaporation, but the difference is related to the depth. As the surface depth increases, the active earth pressure intensity increases nonlinearly, and the flow direction has less influence on it.

A total of 200 sets of strength test data were used to analyze the prediction effects of different models under conventional fly ash content by comparing the calculated values with the experimental values. Further calculate the correlation coefficient ρ of the different calculation models, the residual mean square error δe , and the mean value γ of the ratio between the calculated value of the model and the experimental value. Where ρ represents the consistency between the calculated value of the model and the experimental value, and the larger the ρ is, the higher the correlation between the calculated value of the model and the

experimental value is, and the better the prediction effect of the calculated model is; δe and γ represent the calculated value of the model [10]. The smaller the consistency with the experimental values, the better the agreement between the calculated values of the model and the experimental data; the closer the γ is to 1.0, indicating that the calculated value of the model is closer to the experimental value in general, and the prediction effect of the calculation model is better.

4.2. Strength calculation model

It can be seen from the above test results and analysis that, although the deformation process of the concrete-filled steel tube is complicated, and the loading method is different, the ultimate bearing capacity is not affected by the deformation history. From then on, the strength calculation on the buttocks of the steel pipe can be solved by the limit equilibrium method. The basic assumptions are as follows [11]:

In the limit state, the core coagulation is in a three-way stressed state, the steel bar is in the longitudinal pressure-bad tension biaxial stress state, and the deformation condition of the steel bar has no effect on the ultimate strength of the core concrete; the concrete under three-way compression The strength limit conditions can be described by a large number of experimentally determined equations, and the steel bars are subjected to VonMises yield conditions, so

$$A_s = \pi d_c t \quad (1)$$

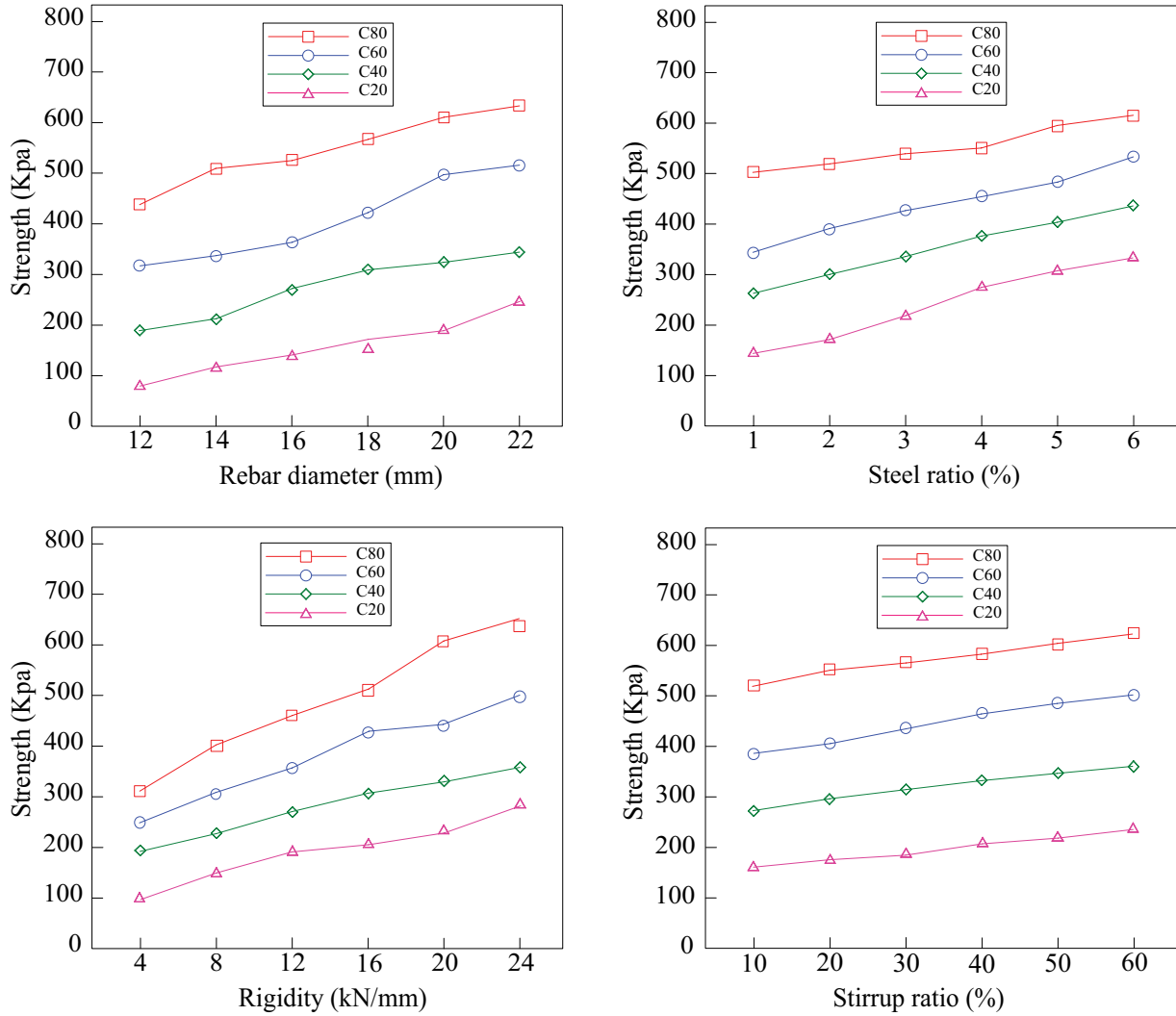


Fig. 5. Relationship between strength and rebar diameter, steel ratio, rigidity, and stirrup ratio.

$$\frac{A_s}{A_c} = \frac{4t}{dc} \quad (2)$$

Here, A_s and A_c are the cross-sectional area of the steel bar, dc is the diameter of the steel bar, and t is the loading force.

From the balance condition of a half-circle of steel bars:

$$\sigma_s t = \frac{dc}{2} \sigma_r \quad (3)$$

Thereby,

$$\sigma_s = \sigma_r \frac{dc}{2t} = \sigma_r \frac{2A_c}{A_s} \quad (4)$$

The third principal stress σ_3 on the reinforcing bars is negligible because of its small value. On the outer wall surface of the steel bar, $\sigma_3 = 0$, on the inner wall surface of the steel bar, $\sigma_2 = \sigma_r$, from Eq. (4), $\sigma_3/\sigma_2 = 2t/dc$, When dc/t is between

20 and 100, σ_3 is only 5%–10% of σ_2 . Steel bars with $D/t > 25$ are usually used. When $\sigma_3 = 0$, according to the stress state distribution, the VonMises yield condition of the steel bar to yield state is:

$$\sigma_1^2 + \sigma_1\sigma_2 + \sigma_2^2 = f_3^2 \quad (5)$$

Substituting Eq. (5) into the above formula,

$$\begin{aligned} N &= A_c \sigma_c + A_s \sigma_s = A_c f_c \left(1 + 1.5 \sqrt{\frac{\sigma_r}{f_c} + 2 \frac{\sigma_r}{f_c}} \right) + \sqrt{A_s^2 f_s^2 - 3 A_c^2 \sigma_r^2} - A_c \sigma_r \\ &= A_c f_c \left[1 + \sqrt{1 - \frac{3}{\phi^2} \left(\frac{\sigma_r}{f_c} \right)^2} + \frac{1.5}{\phi} \sqrt{\frac{\sigma_r}{f_c} + \frac{1}{\phi} \frac{\sigma_r}{f_c}} \phi \right] \end{aligned} \quad (6)$$

According to the condition of $dN/d\sigma_r = 0$, the value of σ_1 corresponding to the maximum load Nu should satisfy the following Eq. (7):

$$\frac{1}{2} \frac{-\frac{6}{\phi^2} \frac{\sigma_r}{f_c}}{\sqrt{1 - \frac{3}{\phi^2} \left(\frac{\sigma_r}{f_c}\right)^2}} + \frac{1.5}{2\phi \sqrt{\frac{\sigma_r}{f_c}}} + \frac{1}{\phi} = 0 \tag{7}$$

Generally, the ferrule index of the reinforced concrete column is between 0.2 and 3. For the convenience of application, the coefficient a can be further taken as 2, so that the error of the Nu value caused by the method is limited, ranging from 19.6% to 14.2%, the average is 1.67%, and the calculation formula is significantly simplified.

In summary, the final form of the calculation formula for the strength of reinforced concrete moisture barrier is:

$$N_c = A_c f_c (1 + \sqrt{\phi} + 1.1\phi) \tag{8}$$

5. Calculation model verification

The anchoring force of the moisture-proof layer concrete is composed of chemical cementing force, mechanical biting force, and frictional resistance. When the ribs embedded in the concrete begin to be pulled, the chemical bonding force between the concrete and the ribs provides the main bonding force. As the load increases, the ribs, and the concrete slide relative to each other, and the chemical bonding force gradually breaks from the loading end to the free end. Due to the small mechanical occlusion force between the light-reinforced steel bars, the moisture-proof layer with weak ribs and the concrete, it is gradually pulled out after slippage [12–14]. Ribbed steel bars or ribbed ribs when the moisture-proof layer is pulled, the flanges of the ribs press the surrounding concrete, which can effectively improve the mechanical bite force and provide a larger anchoring

force after the relative slip occurs (Fig. 6). Therefore, after the relative sloping of the ribbed steel or moisture-proof layer, the oblique anchoring force of the concrete is at an angle α to the direction of the rib, and the force can be decomposed into the resistance along the direction of the rib and the vertical rib. Studies have shown that the ratio of the coefficient of friction of the ribbed steel to the concrete, that is, the ratio of the radial compressive stress to the bond stress is basically a certain value, and α is approximately 45° near the failure. Since the bonding behavior of the “strong rib” moisture barrier is similar to that of steel, the coefficient of friction can be taken. With the increase of the pulling force, the horizontal stress τ of the surface of the rib and the hoop tensile stress produced by the extruded concrete of the ribs increase continuously.

There are many factors affecting the compressive strength of rock similar materials, and there is no clear functional relationship between the influence degree and influence law of each factor. It is necessary and realistic to find or establish a quantitative calculation model with high efficiency and small error to predict the physical and mechanical parameters of similar materials. Dimensional analysis is one of the important means to solve complex phenomena or problems. Through dimensional analysis, it is clear which factors control the compressive strength of similar materials, and the significance of these factors is analyzed, so that it is given mathematically. Try to be as accurate as possible. At the same time, the dimensional analysis method can simplify the experiment, explain the relationship between the quantity and quality of similar materials in the test process, and quantitatively calculate the physical and mechanical parameters of the rock similar material ratio test specimens. When the total amount of the proportioning materials is constant, the compressive strength of similar materials decreases remarkably with the increase of the amount of filling materials (Fig. 7). Water and glycerin are used as binders in similar materials. During the curing process, the cementing material continuously undergoes hydration reaction under the action of the binder. The cementation strength between the coarse aggregates is continuously enhanced, and the hydration products are also filled between the coarse aggregates. The pores make the similar material uniform, stable, and dense. Sand particle size has a significant effect on the water absorption and permeability coefficients of similar materials, and also has a significant effect on the softening coefficient of similar materials. The water properties of similar materials under different sand particle sizes are quite different. The compressive strength of the material is closely related to its hydraulic properties. Therefore, the sand particle size also has a significant influence on the compressive strength of the material [15].

After careful analysis, it is found that the longitudinal reinforcement ratio of the steel-reinforced concrete frame beam is 0.3%, and the reinforcement ratio of the frame beam is not separately specified. Therefore, the software is the reinforcement of the steel frame beam. Rate to configure the longitudinal reinforcement of the frame beam. In the high gauge, the reinforcement ratio of the frame beam and the frame beam is, respectively, specified, and the frame beam reinforcement is larger than the ordinary frame beam.

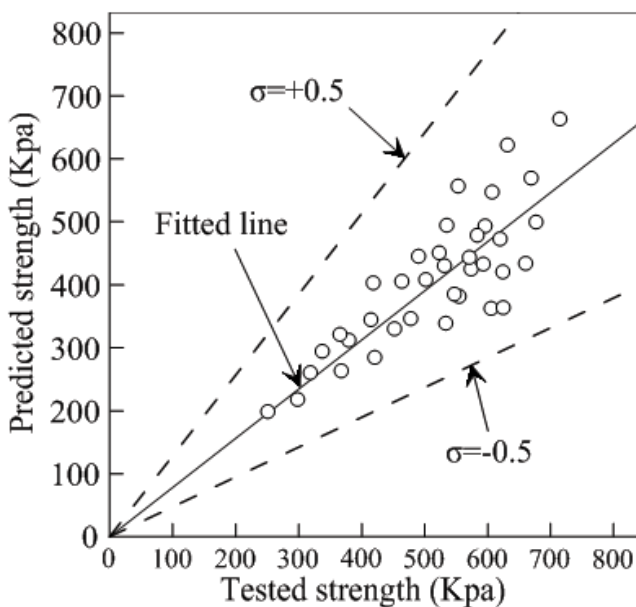


Fig. 6. Comparison of measured and simulated values of strength.

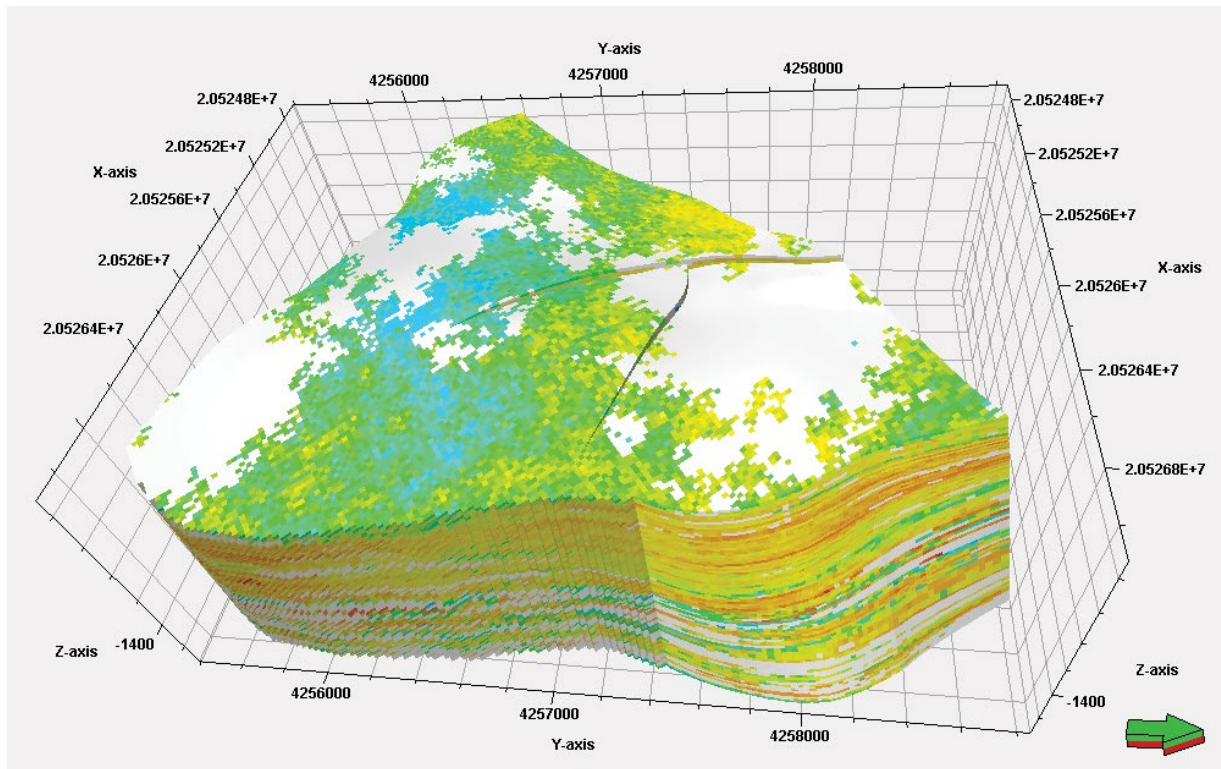


Fig. 7. Finite element simulation results of moisture barrier strength.

The comparative analysis found that in the calculation of the normal section; however, in the calculation of the reinforcement, the reinforced concrete according to the high regulation regulations the calculated internal force of the converted beam under horizontal earthquakes is further increased, while the frame-supported beam is not similarly increased. The frame-supported frame with the steel-reinforced concrete model is significantly better than the ordinary reinforced concrete model in terms of seismic performance, hysteretic behavior, energy dissipation capacity, overall ductility, and stiffness degradation under vertical and horizontal low-cycle repeated loads [16,17]. Due to the contribution of the steel skeleton, the weak layer has moved up, the yield failure mechanism of the whole structure tends to be reasonable, and the plastic rotating ductility of the bottom frame pillar and the frame beam is also significantly improved. Compared with the less stressed reinforced concrete conversion beam, the longitudinal reinforcement has more safety margin; compared with the frame beam is higher. In view of the complexity and importance of the frame beam, in order to ensure its design safety and good seismic performance, the longitudinal reinforcement ratio of the special-grade frame beam of the project is determined to be 0.6% [18–22].

6. Conclusions

A multi-factor model of strength of reinforced concrete moisture barrier under different influencing factors was established. The established model calculation results are consistent with the residual strength degradation law of

concrete and satisfy the boundary conditions, which can effectively simulate the residual strength degradation law of concrete during the fatigue process. Therefore, this paper chooses the strain corresponding to the maximum stress of the softening section of the concrete monotonic static load stress-strain curve as the fatigue failure criterion. It is reasonable and feasible to use the softening section curve to approximate the residual strength envelope of concrete under fatigue failure. Therefore, this paper chooses the strain corresponding to the maximum stress of the softening section of the concrete monotonic static load stress-strain curve as the morphological damage criterion. It is reasonable and feasible to use the softening section curve to approximate the strength calculation model of concrete under loading failure. Based on the boundary condition and strength envelope theory of residual strength theory, the residual strength-stress equation of reinforced concrete subjected to arbitrary loading is derived, and the residual strength calculation model of concrete after any number of loading is established.

The statistical analysis of the compressive strength of the rock similar material specimens was carried out, and the quantitative relationship between the compressive strength and the influencing variables was obtained. Compared with the traditional mechanical test correction model, the long-term test process and the complicated calculation process are omitted, and the prediction efficiency is greatly improved. The residual strength of the concrete obtained by the calculation model is close to linear change, and the test tends to be nonlinear. The root cause is the function introduced and the continuity of the test data. Therefore, the key to the later

research is to introduce a function consistent with the actual damage of the concrete, and the more residual strength test points in the test, the closer the obtained concrete strength degradation law is to the actual. At present, the experimental and theoretical research of reinforced beams mainly focuses on the role of static load, and has little research on the long-term performance after reinforcement, cyclic loading, and the mechanical behavior under corrosive environment; the bearing capacity and strain capacity of reinforced beams. There are relatively many studies, and there is a lack of systematic discussion on the ductility of reinforced beams. These still require further research and analysis from theory and experiment.

References

- [1] Y.Q. Cui, Y.Z. Wang, J. Wang, Analysis on reliability of reinforced concrete structures in marine environment considering resistance time-varying characteristic, *J. Waterw. Harbor*, 34 (2013) 106–112.
- [2] R.K. Guo, Y.C. Tang, X.W. Rao, Ultimate strength analysis of damaged reinforced concrete columns strengthened with FRP, *Struct. Eng.*, 34 (2018) 142–148.
- [3] L. Zhou, X.P. Tan, Y.Q. Wang, G. Shi, The calculated model research on bearing capacity of axially loaded steel columns strengthened by enclosed reinforced concrete while under load, *Ind. Constr.*, 47 (2017) 18–22.
- [4] B.J. Si, Z.G. Sun, Q.H. Ai, Application of SOLID65 element in the finite element analysis of concrete structures, *Ind. Constr.*, 37 (2007) 87–92.
- [5] M. Rezaei, A. Mostafaeipour, M. Qolipour, H. Arabnia, Hydrogen production using wind energy from sea water: a case study on southern and northern coasts of Iran, *Energy Environ.*, 29 (2018) 333–357.
- [6] M.N. Sultana, S. Akib, M.A. Ashraf, Thermal comfort and runoff water quality performance on green roofs in tropical conditions, *Geol. Ecol. Landscapes*, 1 (2017) 47–55.
- [7] X.R. Xiang, Empirical formula for compressed strength of cement-soil in soft soil ground, *Ind. Constr.*, 45 (2015) 844–847.
- [8] B.A. Fonge, P.T. Tabot, M.A. Bakia, C.C. Awah, Patterns of land-use change and current vegetation status in peri-urban forest reserves: the case of the Barombi mbo forest reserve, Cameroon, *Geol. Ecol. Landscapes*, 3 (2019) 104–113, doi: 10.1080/24749508.2018.1508981
- [9] A. Amamra, K. Khanchoul, Water quality of the Kebir watershed, northeast of Algeria, *J. Clean WAS*, 3 (2019) 28–32.
- [10] S. Thiruchelvam, R.S. Muda, A. Ghazali, F.F. Norkhairi, K.N. Mustapha, N. Yahya, R. Sulaiman, Z. Che Muda, Inception of 3ES in promoting disaster resilient communities living near hydropower dams of Peninsular Malaysia, *Malaysian J. Geosci.*, 2 (2018) 17–21.
- [11] N.S. Zafisah, W.L. Ang, A.W. Mohammad, Cake filtration for suspended solids removal in digestate from anaerobic digested palm oil mill effluent (Pome), *Water Conserv. Manage.*, 2 (2018) 05–09.
- [12] E. Masri, M.D.M. Samsudin, Optimization performance of biological cathodic protection system using organic waste, *Environ. Ecosyst. Sci.*, 2 (2018) 25–29.
- [13] K. Li, S.Y. Li, X.L. Wang, Study on calculation model of interfacial debonding bearing capacity of the CFRP-concrete interface based on beam tests, *Struct. Eng.*, 33 (2017) 40–46.
- [14] Q. Chen, G.L. Guo, Active earth pressure strength model of unsaturated soil, *J. Heilongjiang Univ. Sci. Technol.*, 26 (2016) 700–704.
- [15] Y.F. Zhao, J. Q. Zhao, L.F. Yang, Z. Chen, Multifactor computational model for strength of concrete with high fly ash content, *Bull. Chin. Ceram. Soc.*, 37 (2018) 2941–2953.
- [16] S.H. Cai, Z.S. Jiao, Behavior and ultimate strength of short concrete-filled steel tubular columns, *China Acad. Build. Res.*, 6 (1984) 13–29.
- [17] H. Ben Mariem, M. Chaieb, Climate change impacts on the distribution of *Stipa tenacissima* l. Ecosystems in North African arid zone - a case study in Tunisia, *Appl. Environ. Res.*, 15 (2017) 67–82.
- [18] A. Lugo-Vazquez, M.R. Sanchez-Rodriguez, J. Morlan-Mejia, L. Peralta-Soriano, E.A. Arellanes-Jimenez, M.A. Escobar-Oliva, M.G. Oliva-Martinez, Ciliates and trophic state: a study in five adjacent urban ponds in Mexico City, *J. Environ. Biol.*, 38 (2017) 1161–1169.
- [19] D.Y. Gao, D. Fang, H.X. Gu, Bonding mechanism and strength calculation model of GFRP-steel composite rebars embedded in concrete, *J. Build. Struct.*, 39 (2018) 130–139.
- [20] Z. Yue, Y.C. Ye, Q.H. Wang, N. Yao, Y.B. Shui, A model for calculation of compressive strength of rock-like materials based on dimensional analysis, *Rock Soil Mech.*, 39 (2017) 216–228.
- [21] G.E. Devora Isiordia, A. Robles Lizarraga, G.A. Fimbres Weihs, J. Alvarez Sanchez, Comparison of discharge methods for spill of brines, from a desalination plant in Sonora, Mexico, *Rev. Int. Contam. Ambiental*, 33 (2017) 45–54.
- [22] X.F. Jin, Y.Z. Yu, C.X. Huang, L.D. Ma, Design of steel reinforced concrete frame transfer structure for out-of-code high-rise residential building, *Build. Struct.*, 49 (2019) 90–95.